Strojniški vestnik - Journal of Mechanical Engineering 70(2024)11-12, 595-606
DOI:10.5545/sv-jme.2024.1076
Original Scientific Paper
Received for review: 2024-06-27
Received revised form: 2024-10-04
Accepted for publication: 2024-10-21

Experimental Investigation on SS202 using Tubular and Double D Tubular Electrode Tool in Electrical Discharge Drilling Machining

Manikandaprabu Pandiyan[1,*] – Saravanan Kanthasamy Ganesan[2]
Department of Mechanical Engineering, Sona College of Technology, , Salem-636005, Tamil Nadu, India

To meet the demands of the manufacturing industry, a more robust approach is needed for current manufacturing processes. Machining of very hard materials with excellent dimensional accuracy and surface integrity is a challenging task, Currently, the electrical discharge machining (EDM) process is the optimal solution for machining such materials. Electrical discharge drilling machines find applications in various sectors such as aerospace, automobile and medicine. In this research, two different brass electrode geometries are considered: tubular electrode tool (TET) and double D tubular electrode tool (DDTET) on an SS202 work-piece. The input parameters of peak current (PI), pulse time ON (PONT), and pulse time OFF (POFFT) were varied. The output response measured and compared were material removal rate (MRR) and over cut (OC). The Taguchi technique was used to design the I16 orthogonal array (OA) experiment, and analysis of variance (ANOVA) was employed for result analysis using Minitab20 statistical software package. The results showed that the DDTET method produced significantly better MRR and OC improvements of 21.66 % and 2.28 % respectively. Additionally, a study was conducted on the formation of the recast layer (RL) and the heat affected zone (HAZ).

Keywords: modified electrode geometry, material removal rate, over cut, heat affected zone, recast layer, analysis of variance

Highlights

- *A novel tool (DDTET) geometry was designed and utilized to perform drilling operations on SS 202 material.*
- *The performance of the novel tool was compared to that of a conventional tool, based on response characteristics such as MRR, OC, HAZ, and RL.*
- *Taguchi and ANOVA methods were employed to identify the optimal performance outcomes.*
- *The PONT input parameter demonstrated superior performance in terms of MRR and OC for both TET and DDTET geometries.*
- *A study on RL and HAZ was conducted using scanning electron microscope (SEM) imaging.*

0 INTRODUCTION

EDM is a non-conventional manufacturing process utilized for precision material removal. This technique involves immersing an electrically conductive work-piece and a tool, known as an electrode, in a dielectric fluid. Upon applying a potential difference between the work-piece and the electrode, controlled electrical discharges occur, leading to localized melting and vaporization of the work-piece material. This phenomenon enables precise shaping of intricate geometries in materials that are traditionally challenging to machine. EDM finds application in industries such as aerospace, automotive, and medicine, where high precision and complex component fabrication are required. R. Kirubagharanet et al. **[1]** conducted drilling operations using electrical discharge drilling (EDD) on Inconel X750 utilizing a modified square electrode tool. The results of the experiment demonstrated enhancements of 12 % in MRR, 9 % in SR, and 11 % in EWL. Pal et al. **[2]** conducted an experiment on SS310 and SS316 using EDD, considering input parameters such as V voltage [V], C capacitance [pF], $PONT$ [µs], and $POFFT$ [µs]. The findings of the study indicated that the optimum machining conditions for SS310 steel were identified as V = 150 V, C = 100 pF, $PONT$ = 30 µs , and $POFFT$ = 20 µs. Conversely, for SS316 steel, the optimal parametric conditions were found to be V = 200 V, C = 1000 pF, $PONT$ = 20 µs, and $POFFT$ = 25 µs using the Taguchi approach. Yadav et al. **[3]** conducted a study utilizing EDD on a copper work-piece, considered input parameters such as voltage, feed rate, and powder concentration in the dielectric fluid. The ANOVA results from this investigation revealed that voltage contributed 93.5 % of the MRR, 58.24 % of the tool wear rate (TWR), and 67.3 % of the aspect ratio (AR). Chaudhari et al. **[4]** conducted EDD on Ni55.8Ti alloy employing a graphite electrode tool. The results of this experiment showed enhancements of 76.91 %, 38.40 %, 34.36 %, and 44.54 % for MRR, TWR, SR, and dimensional deviation (DD), respectively. Manikandan et al. **[5]** performed EDD on a Si3N4–TiN ceramic composite with a copper electrode. The findings indicated enhancements in MRR by 0.0354 gm/min and TWR by 0.001035 gm/min Shabarinathan et al. **[6]** performed an EDM process on Inconel using an aluminum composite electrode. Their experiments identified the optimal process parameter for MRR at a

*Corr. Author's Address: Department of Mechanical Engineering, Sona College of Technology, Salem - 636005, India, maniprabujkpm@gmail.com

current of 12 A, beyond which the MRR declined due to plasma channel expansion. The optimal PONT was determined to be 8 μs, with a POFFT of 4 μs. Sawant et al. [7] performed EDD on Ti–6Al–4V alloy utilizing copper (Cu), tungsten copper (WCu), and tungsten carbide (WC) electrodes. The results revealed that the MRR achieved with the WCu electrode was 6.11 % higher than that with the Cu electrode and 21.92 % higher than that with the WC electrode. Selvarajan et al. [8] conducted an experiment involving EDD on molybdenum disilicide–silicon carbide composites, employing copper electrodes. The outcomes highlighted that the primary machining parameters were determined to be current (34.6749 %), PONT (25.6502 %), and gap voltage (12.0462 %). Rafaqat et al. [9] developed a modified triangular cross-section copper electrode for the EDD process on D2 steel. They observed notable outcomes, including a 32.6 % enhancement in MRR, a reduction of 20.6 % in overcut (OC), and a significant decrease of 72.5 % in taper angle (TA). Rafaqat et al. [10] fabricated copper tools with various cross-sectional geometries for use in the EDM process. Their results showed an improved MRR of 317.24×10^6 ($\mu m^3 s^{-1}$) compared to traditional tool geometries. Kumar and Singh [11], Shah and Saha [12], and Saha et al. [13] conducted EDM experiments using a modified solid electrode tool, featuring slotted, cylindrical and conical shapes for the tool's outer profile. Ji et al. [14] carried out EDM experiments using a helical-profiled TET. Yadav et al. [15] conducted EDM experiments with various straight grooved tool profiles and a helical-shaped tool in TET.

From the literature reviewed, it is evident that global research on EDM has focused on enhancing MRR, SR, EWL, DD, and OC accuracy. Although various flushing methods and tool designs have been employed to enhance MRR, dimensional accuracy, and other factors, further in-depth studies are needed to fully understand the EDM process. This research investigates two different electrode geometries, TET and DDTET, focusing on their effects on MRR and AD. The findings reveal that the DDTET electrode has a significant impact on both MRR and AD.

1 METHODS

A novel tool geometry was designed and utilized to perform drilling operations on SS 202 material using EDM. The performance of this novel tool was compared to a conventional tool, focusing on key response characteristics: MRR, OC, HAZ, and RL. Taguchi, surface response methodology, contour plots and ANOVA methods were employed to identify the optimal performance outcomes, ensuring a thorough statistical analysis of the results.

Additionally, an in-depth study on the RL and HAZ was conducted using SEM imaging. The RL was generated in the sparking zone, where localized heating of a thin layer of the work-piece occurred. The high temperature caused the formation of a molten layer, which solidified during the subsequent quenching process, leading to the creation of the RL. Due to the low thermal conductivity properties of SS202 material, a tempered layer was formed below the RL, referred to as the HAZ [16]. This allowed for a detailed examination of the microstructural changes and quality of the drilled holes, providing insights into the efficacy of the novel tool geometry in minimizing defects and enhancing the overall drilling performance.

2 EXPERIMENTAL

2.1 Experimental Setup

The experiments to drill the SS202 work-piece were performed using the Suzhou Baom electrical discharge drilling machine (EDDM) with various settings for *PI*, *PONT*, and *POFFT*. The machine has an adaptive Z-axis movement and automatically adjusts the arc gap between the work-piece and the electrode tool. The spindle rotational movement was maintained at 110 rpm, and the dielectric fluid pressure, supplied by an electrically assisted pump, was kept constant at 1 MP, while the electrode tool with a 3 mm outer diameter and 1 mm hole diameter was fixed as negative polarity and the work-piece as positive polarity. The EDDM is capable of adapting to various electrode diameters from 0.3 mm to 3 mm. The dielectric fluid, deionized water, is provided to the work area through a reservoir connected to a filter system, pump, and pressure adjustment valve. The ionization process in the work area produced etching at about 8,000 °C to 10,000 °C. The EDDM is illustrated in Fig. 1. The SS202 material, which is widely used in high-speed aerospace motor housing, automotive trim, railway carriages, trailers, fluid filters, and water clams, was chosen due to its high hardness, good corrosive resistance, and durability. Detailed specifications of the EDDM machine and SS202 material composition are given in Tables 1 and 2, respectively.

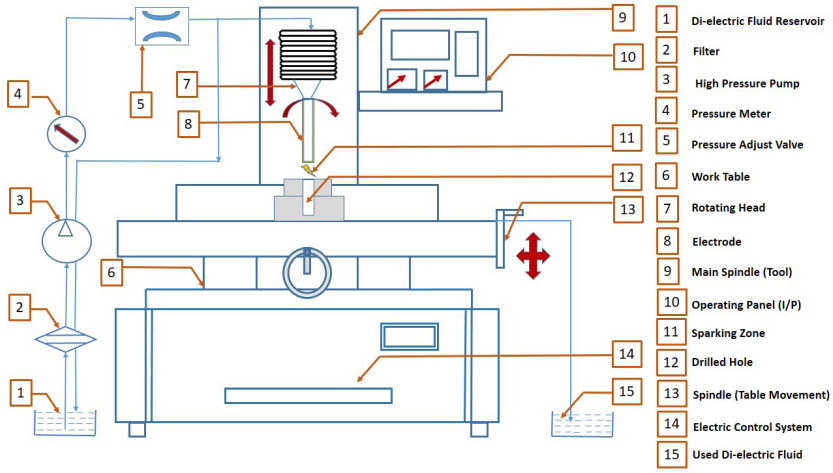

Fig. 1. *Experimental setup*

Table 1. *EDDM machine specification*

No	Specification	Range
1	Supply power	3 Phase
2	Maximum voltage	415 V; AC
3	Frequency	45 Hz
4	Axis travel (X, Y, Z)	400 mm × 300 mm × 300 mm
5	Rated power	35 kVA
6	Weight	650 kg
7	Rated current	35 A

Table 2. *SS202 Material Composition* [24]

No	Element	Content [%]
1	Iron (Fe)	68
2	Chromium (Cr)	17 to 19
3	Manganese (Mn)	7.50 to 10
4	Nickel (Ni)	4 to 6
5	Silicon (Si)	≤ 1
6	Carbon (C)	≤ 0.15
7	Phosphorous (P)	≤ 0.060
8	Sulphur (S)	≤ 0.030
9	Nitrogen (N)	≤ 0.25

2.2 Construction of DDTET

The brass electrodes used in the experiment were tubular in shape, with an outer diameter of 3 mm and a hole diameter of 1 mm. The hole allowed the pressurized dielectric fluid to enter the machining area. This standard electrode is called the TET geometry, as depicted in Fig. 2a. Brass was chosen as the material for the tool due to its high conductivity property. A modified version of the novel DDTET geometry was designed for the drilling process, as shown in Fig. 2b. The DDTET was fabricated using a wire electrical discharge machining machine (Concord Wire EDM, India). The modified tool dimension was reduced by 350 microns on one side, and the same amount was reduced in the opposite direction, which increased the gap between the electrode and work-piece. Lo et al. [17] and Malayath et al. [18] conducted an EDD process on carbon steel using a slotted copper electrode. This increased gap resulted in an improvement in MRR by 120 % to 153 %, as well as enhanced specimen precision and dimensional accuracy. Both the standard TET and DDTET were used to drill the SS202 work-piece material.

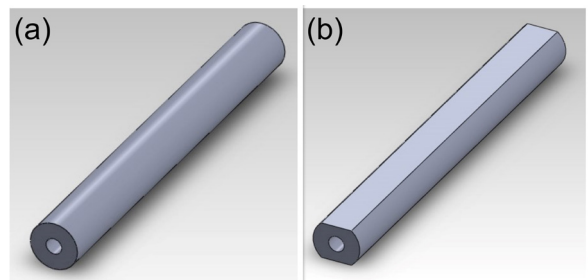

Fig. 2. *a) Model of TET, and b) model of DDTET*

2.3 Experimental Design Using Taguchi Method

The PI, PONT, and POFFT values were selected as 4 A, 5 A, 6 A, and 7 A; 3 µs, 4 µs, 5 µs, and 6 µs; and 5 µs, 6 µs, 7 µs, and 8 µs, respectively, through trial runs and prior experimental investigations. The experiments were designed using the Taguchi method [19]. Three variables, each at four levels, were utilized, resulting in a degree of freedom calculation of 3(4-1) = 9. Consequently, an L16 OA, which exceeds the

required 9 degrees of freedom, was selected and is presented in Table 3.

Table 3. *Machining parameters of L16 RO*

Run order (*RO*)	*PI* [A]	*PONT* [μs]	*POFFT* [μs]
1	4	3	5
2	4	4	6
3	4	5	7
4	4	6	8
5	5	3	6
6	5	4	5
7	5	5	8
8	5	6	7
9	6	3	7
10	6	4	8
11	6	5	5
12	6	6	6
13	7	3	8
14	7	4	7
15	7	5	6
16	7	6	5

The Taguchi ratio is a transformed value derived by subtracting the experimental value from the target value. The signal/noise (SN) ratio is calculated by dividing the mean by the standard deviation and is used to measure the quality of the output. The SN ratio is categorized by Taguchi into three groups, namely 'larger is better', 'nominal is better', and 'smaller is better', depending on the nature of the response [20]. In the present experimental study, MRR were considered as 'larger is better' (Eq. (1)) response characteristic and *OC* considered as 'smaller is better' (Eq. (2)). The Minitab20 statistical software package was employed for the Taguchi experimental design, mean graph analysis, *SN* ratio graph analysis, analysis of variance (ANOVA) results, surface plots, and contour plots.

$$SN = -10\log_{10}\left[\Sigma\left(\frac{1}{y^2}\right)\Big/ n\right], \tag{1}$$

$$SN = -10\log_{10}\left[\Sigma\left(y^2\right)/ n\right]. \tag{2}$$

2.4 Experimental Analysis Using ANOVA Method

ANOVA was employed to examine the statistical outcomes of the TET and DDTET geometries. It aimed to identify the input parameters that had a more substantial impact on the machining process and determine the extent of their influence. Input parameters with a p-value less than 0.05 were considered significant at a 95 % confidence level.

2.5 Measurement of MRR

The 3 mm thick work-piece was drilled using EDDM, where three different drilling methods were typically available, as illustrated in Fig. 3. In this study, the normal drilling method, shown in Fig. 3b was selected. TET and DDTET electrode tools were used, each responsible for 16 holes, totaling 32 holes on the SS202 material. Drilled holes were represented by yellow and pink circles for TET and DDTET respectively as shown in Fig. 4. MRR was calculated using the weight reduction method (Eq. (3)), where initial and final weights of the work-piece (Wi and Wf), density (ρ), and machining time (t) are considered [21] and [22].

$$MRR = \frac{W_i - W_f}{\rho \times t} \quad \left[\mathrm{m^3\ min^{-1}}\right]. \tag{3}$$

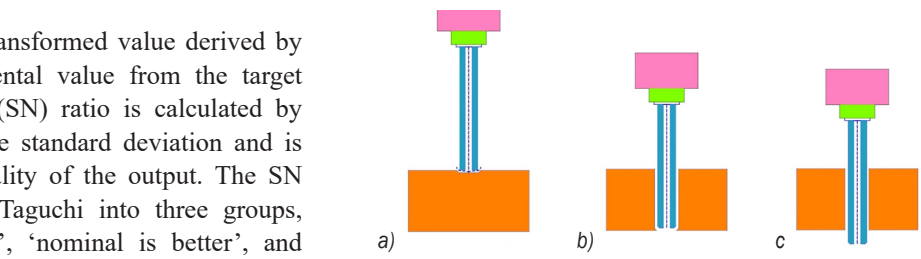

Fig. 3. *Drilling types; a) approach drilling, b) normal drilling, and c) break-through drilling*

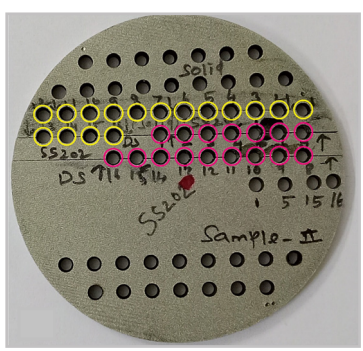

Fig. 4. *Drilled holes on SS202 work-piece*

$$OC = \left[\frac{d1 + d2 + d3 + d4}{4}\right] \quad [\mathrm{mm}], \tag{4}$$

$$CoP = \left[\frac{\left|V_{\max} - V_{\min}\right|}{\left(V_{\max} + V_{\min}\right)/2}\right] \times 100 \quad [\%], \tag{5}$$

where $V_{\max}$ is maximum value and $V_{\max}$ minimum value.

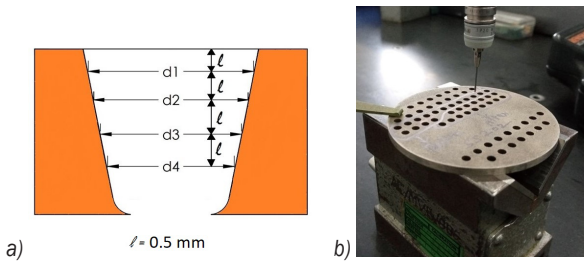

Fig. 5. *a) Depth of OC measurement, and b) measurement of OC using CMM*

2.5 Measurement of *OC*

The *OC* measurement was conducted using a co-ordinate measuring machine (CMM) (RENISHAW MCU lite-2, United Kingdom). A multiple point touching method was employed to determine the *OC* value as shown in Fig. 5b, with the *OC* measured at four different depths: 0.5 mm (*d*1), 1 mm (*d*2), 1.5 mm (*d*3), and 2 mm (*d*4) as shown in Fig. 5a. Eq. (4) was used to calculate the OC value. The change in percentage (*MRR* and *OC*) presented in Table 4 was determined using Eq. (5) **[22]**.

$$MRR = -4.9 + 13.80\,PI + 8.99\,PONT - 13.67\,POFFT - 0.611\,PI \times PI - 0.022\,PONT \times PONT + 0.645\,\mathrm{POFFT} \times \mathrm{POFFT}, \quad [\mathrm{mm^3 min^{-1}}] \qquad (6)$$

$$OC = 2.8166 + 0.04051\,PI + 0.00333\,PONT + 0.02395\,POFFT - 0.003875\,PI \times PI + 0.000213\,PONT \times PONT - 0.001587\,POFFT \times POFFT \quad [\mathrm{mm}], \qquad (7)$$

3 RESULTS AND DISCUSSION

3.1 Comparison Study with TET and DDTET Geometry

3.1.1 MRR Comparison Study

Table 4 highlights notable trends in *MRR* for both *TET* and *DDTET* geometries. The 9th RO (*consider the following input arrangement for the forthcoming RO) (*PI = 6 A, $PONT$ = : 3 µs, $POFFT$ = 7 µs) with low $PONT$ = 3 µs in the TET geometry resulted in decreased *MRR* due to reduced pulse live time. Even increasing *PI* with low PONT didn't significantly improve *MRR*. In contrast, the DDTET geometry's 1st RO (*4 A, 3 µs, 5 µs) had minimized MRR due to lower experimental parameters, resulting in less energy distribution and sparking time. The 16th RO (*7 A, 6 µs, 5 µs) for both geometries showed improved *MRR* due to parameters set in a peak trend, enhancing material removal with increased thermal energy distribution. The change of electrode gap between the tool and work-piece had minimal effect on change of *MRR* 2.26 % at 3rd RO (*4 A, 5 µs, 7 µs), and the 9th

Table 4. *MRR and OC of TET and DDTET geometry*

RO	TET geometry *MRR* [mm³min⁻¹]	DDTET geometry *MRR* [mm³min⁻¹]	Change of *MRR* [%]	*OC* of TET geometry [mm]	*OC* of DDTET geometry [mm]	Change of *OC* [%]
1	14.76135	15.1400	2.5326	3.0499	3.0083	1.37
2	17.93606	18.4803	2.9889	3.0627	3.0191	1.43
3	21.175	21.6594	2.2618	3.0811	3.0286	1.72
4	22.47238	23.1102	2.7985	3.0992	3.0349	2.10
5	17.03451	18.8571	10.1561	3.0635	3.0189	1.47
6	27.78822	30.1863	8.2729	3.0662	3.0209	1.49
7	26.4138	27.4010	3.6688	3.0860	3.0324	1.75
8	34.00262	36.4855	7.045	3.0965	3.0417	1.79
9	14.42659	17.9304	21.658	3.0662	3.0227	1.43
10	24.15692	26.1635	7.9752	3.0836	3.0257	1.90
11	42.26533	45.0064	6.2817	3.0784	3.0231	1.81
12	46.45681	50.1515	7.6488	3.0928	3.0332	1.95
13	16.78942	18.5702	10.0724	3.0763	3.0128	2.09
14	30.07439	32.1693	6.7313	3.0773	3.0183	1.94
15	44.81558	46.4048	3.4843	3.0836	3.0178	2.16
16	62.87964	66.8733	6.1558	3.0865	3.0168	2.28

RO (*6 A, 3 µs, 7 µs) had the highest change of MRR 21.66 % percentage change between TET and DDTET geometries. This suggests that increasing the annular gap significantly improved MRR at the 9th RO due to increased ionization potential.

3.1.2 *OC* Comparison Study

Table 4 shows that the 1st RO (*4 A, 3 µs, 5 µs) resulted in a reduced *OC* for both TET and DDTET geometries due to a downward trend in all experimental input parameters, indicating that low current intensity, low *PONT*, and low *POFFT* reduces ionization in the machining zone, resulting in a decreased *OC*. Conversely, the 4th RO (*4 A, 6 µs, 8 µs) in the TET geometry and the 8th RO (*5 A, 6 µs, 7 µs) in the DDTET geometry had an increased *OC*, indicating that higher *PONT* along with increased ideal timing (*POFFT*), increase the ionization potential at the machining zone and result in a larger hole size.

Table 4. Showing that the 1st RO (*4 A, 3 µs, 5 µs) had the least deviation percentage between TET and DDTET geometry, indicating that changing the annular gap had little effect on *OC* deviation. In contrast, the 16th RO (*7 A, 6 µs, 5 µs) had the highest deviation of (2.28 %), indicating that the maximum distance between the tool and work-piece, significantly affected *OC* deviation at 16th RO.

3.2 *SN* Ratio and Mean Graphs for TET and DDTET Geometries

3.2.1. *MRR* Comparison Study Using *SN* Ratio and Mean Graphs

Figs. 6 and 7 depict graphs of the TET and DDTET geometries respectively which followed the same contour pattern. *PI* and *PONT* positively impact *MRR*, indicating that higher values result in more efficient material removal. Conversely, increasing *POFFT* reduces *MRR* due to longer intervals between electrical discharges, which decreases thermal distribution within the work-piece, hindering material removal. These findings emphasize the importance of optimizing input parameters for enhanced drilling efficiency. The Taguchi research showed a mean *R*-Squared (*R-Sq*) value of 98.06 % and an adjusted *R*-Squared (*R-Sq(adj)*) value of 95.16 % for the TET geometry. For the DDTET geometry, the *R-Sq* and *R-Sq(adj)* values were 98.11 % and 95.26 %, respectively. These values indicate that the results closely followed the regression line.

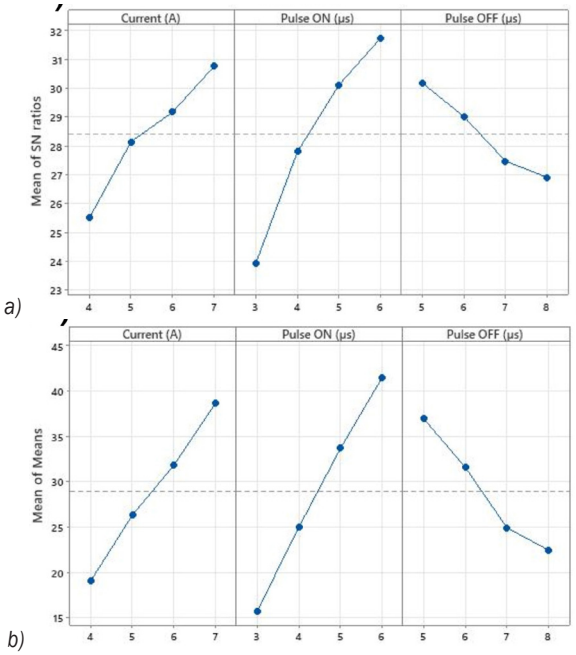

Fig. 6. *a) TET geometry's SN ratio and b) means graph*

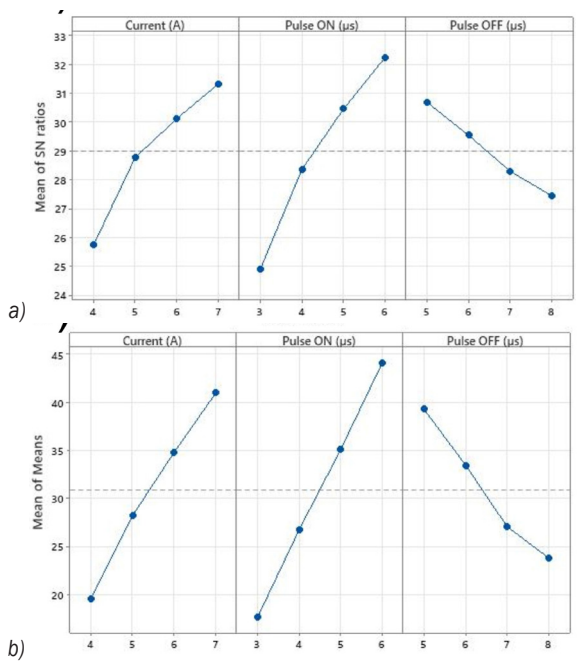

Fig. 7. *a) DDTET geometry's SN ratio and b) means graph*

Based on the Taguchi analysis *PONT* was the most significant factor for both TET and DDTET geometries, indicating that increasing sparking time improves *MRR*. *PI* was the second most significant factor, with increased input resulting in peak thermal energy in the work zone and an increased *MRR* value due to the maximized etching process. *POFFT* was found to be the least significant factor, with a peak

POFFT value reducing energy distribution time and leading to decreased material etching from the machining zone.

3.2.2. *OC* Comparison Study Using *SN* Ratio and Mean Graphs

Fig. 8 shows that in TET geometry a decreased *PI* leads to a lower *OC* value due to lower electron intensity limiting ionization, resulting in minimal heat generation and material etching. Lower *PONT* minimizes current flow time and etching, creating a smaller working area diameter. A lower *POFFT* further reduces material removal and hole diameter. Fig. 9 indicates that in DDTET geometry a maximum *PI* reduces *OC* due to increased distance between the tool and work-piece, regulating ionization. Initially, reducing *PI* decreases *OC*, but further increases in *PI* first raise and then reduce *OC* again. In TET geometry, the *R-Sq* and *R-Sq*(*adj*) values of 97.92 % and 94.79 % show a good fit of the regression line using the Taguchi technique. For the means, *R-Sq* is 99.04 % and *R-Sq(adj*) is 97.61 %, indicating a close match to experimental values in DDTET geometry.

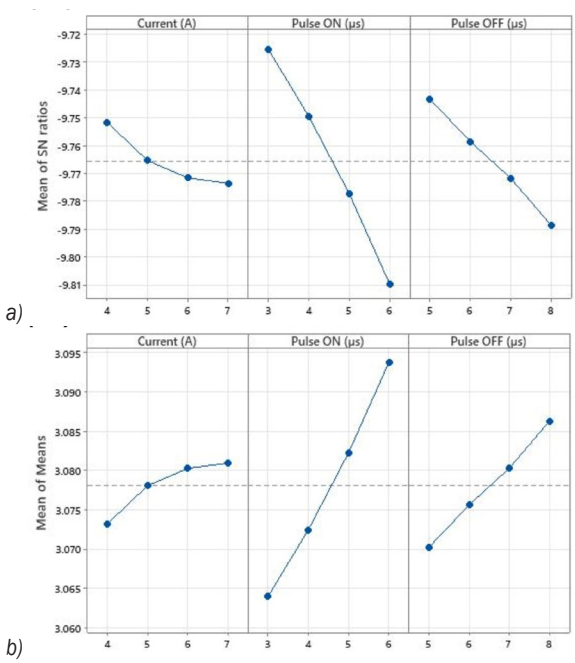

Fig. 8. *a) TET geometry's SN ratio and b) means graph*

Based on the Taguchi analysis, *PONT* is the most significant input parameter affecting *OC* values for both TET and DDTET geometries. In TET geometry, POFFT is the second most significant factor. In contrast, in DDTET geometry, *PI* is the second most significant factor due to the additional gap between the tool and work-piece, which requires higher current intensity to achieve the desired hole diameter. *PI* is the least significant factor in TET geometry, while in DDTET geometry, the least significant input is POFFT.

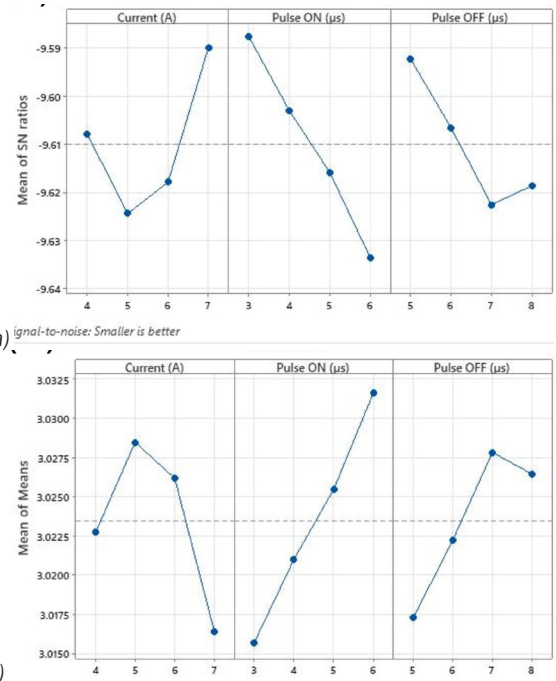

Fig. 9. *a) DDTET geometry's SN ratio and b) means graph*

3.3 Comparison Study of MRR and OC Using Bar Chart

Fig. 10 shows that the DDTET geometry of the modified tool achieved better *MRR* than the TET geometry. The increased annular gap in the DDTET geometry allowed for better debris evacuation, leading to faster electron movement from the electrode tool to the work-piece and improved thermal energy distribution, resulting in increased MRR. In contrast, the TET geometry had a high volume of debris in the machining zone, which increased the likelihood of electron restriction and decreased etching from the tool approaching zone, resulting in reduced *MRR*.

Fig. 11 revealed that the DDTET model achieved that lower *OC* than the TET model, with the minimal distance between tool and work-piece (TET) increasing ionization and thermal energy in the machining zone. Malayath et al. [18] conducted EDM micro end milling using both the electrode and work-piece as WC. They found that a reduced annular gap increases debris concentration, dielectric fluid conductivity, secondary sparking, and material

removal at the side wall. Conversely, an increased distance between electrode and work-piece (DDTET) limits ionization and reduces material etching at the side wall compared to the TET method.

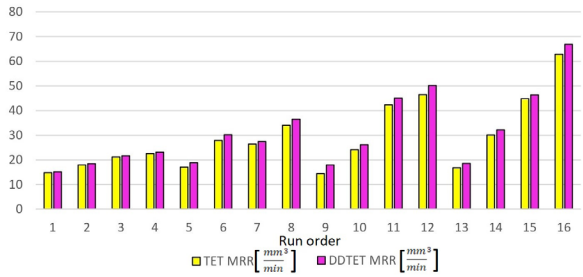

Fig. 10. *MRR chart comparison between TET and DDTET geometry*

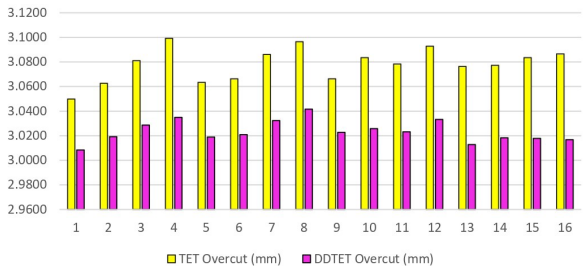

Fig. 11. *OC chart comparison between TET and DDTET geometry*

3.4 ANOVA Analysis

3.4.1 *MRR* Comparison Study Using ANOVA Analysis

Table 5 shows, in the ANOVA result, that *PONT* was the most significant factor in both TET and DDTET geometries, with a contribution of 51.35 % and 48.58 % respectively. Increased sparking time led to improved etching and increased *MRR*. *PI* contributed 28.77 % in the TET geometry and 31.67 % in the DDTET geometry, while *POFFT* had a contribution of 17.95 % and 17.85 % in TET and DDTET respectively for *MRR*. Table 5 shows that the contribution percentages of each input factor for *MRR* in both the TET and DDTET geometries had minimal deviations, indicating that the impact of each factor remained consistent throughout the experiments.

3.4.2. *OC* Comparison Study Using ANOVA Analysis

Table 5 shows that in TET geometry, *PONT*, *POFFT*, and *PI* contributed 72.25 %, 20.33 %, and 5.33 %, respectively, to *OC*. In DDTET geometry, *PONT*, *PI*, and *POFFT* contributed 47.37 %, 28.37 %, and 23.30 %, respectively, to *OC*. The contribution of *PONT* to *OC* decreased by 24.88 % in DDTET geometry, indicating that the reduced annular gap enhances *PONT*'s influence in TET geometry. The *PI* contribution decreased by 23.04 % in the TET model, suggesting that a larger gap increases *PI*'s contribution to *OC* in DDTET geometry. The percentage of deviation (*PoD*) for *POFFT* was 2.97 %, indicating that the change in the annular gap does minor impact to *POFFT's PoD* for *OC*.

Table 5. *Contribution of input factors using ANOVA*

Response	Geometry	*PONT* [%]	*PI* [%]	*POFFT* [%]
MRR	TET	51.35	28.77	17.95
	DDTET	48.58	31.67	17.85
	% of deviation	2.77	–2.90	0.10
OC	TET	72.25	5.33	20.33
	DDTET	47.37	28.37	23.30
	% of deviation	24.88	–23.04	–2.97

3.4.3 DDTET Regression Equation

$$MRR = -4.9 + 13.80\,PI + 8.99\,PONT - 13.67\,POFFT - 0.611\,PI \times PI - 0.022\,PONT \times PONT + 0.645\,POFFT \times POFFT\ [\mathrm{mm^3 min^{-1}}], \quad (6)$$

$$OC = 2.8166 + 0.04051\,PI + 0.00333\,PONT + 0.02395\,POFFT - 0.003875\,PI \times PI + 0.000213\,PONT \times PONT - 0.001587\,POFFT \times POFFT\ [\mathrm{mm}]\,. \quad (7)$$

3.5 Surface and Contour Plots Analysis

3.5.1 Comparison Study of MRR Using Surface and Contour Plots

Figs. 12 and 13 illustrate that higher values of *PI* = 7 A and *PONT* = 6 µs lead to an enhanced *MRR* in *EDD*. In contrast, lower values of these parameters and an increase in spark idling time result in a reduction in *MRR*. Moreover, it is observed that a combination of high *PONT* = 6 µs and low *POFFT* = 5 µs values also contribute to an increase in *MRR*. This is likely due to the extended pulse generation time, leading to heightened ionization in the machining zone, thus facilitating material removal. Notably, both the TET and DDTET geometries exhibit consistent responses to variations in these input parameters, reinforcing the observed patterns in *MRR*.

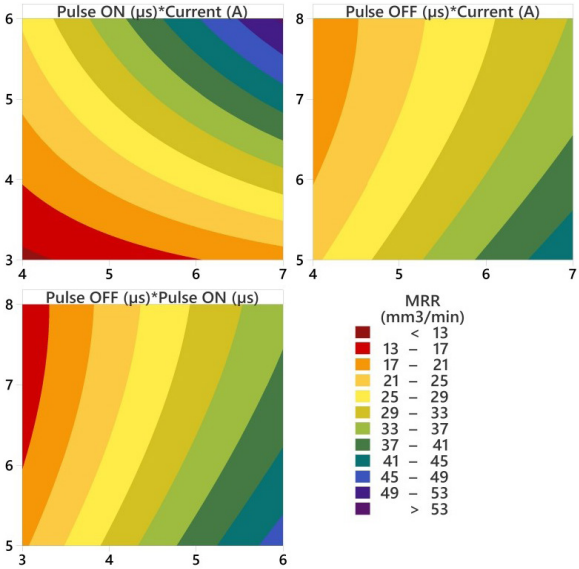

Fig. 12. *MRR Surface plot of TET geometry*

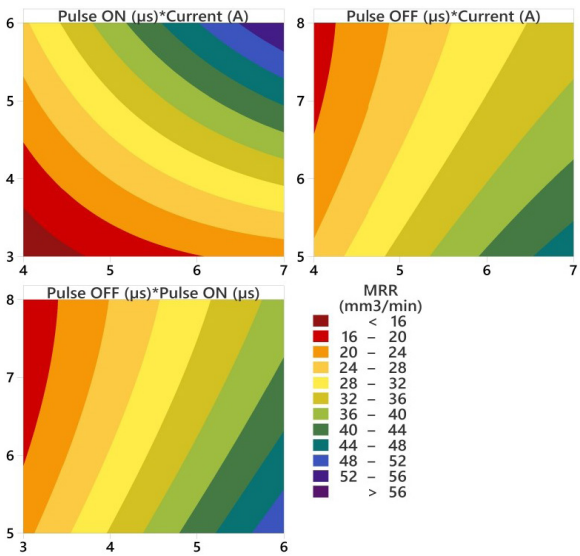

Fig. 13. *MRR Surface plot of DDTET geometry*

3.5.2 Comparison Study of OC Using Surface and Contour Plots

Fig. 14 illustrate that the most significant combinations for achieving smaller *OC* values were lower *PONT* and low-level *PI*. The second most significant combination involved low *POFFT* and low-level *PONT*. Additionally, it revealed that the optimal input values for minimizing *OC* in TET geometry were *PONT* at 3 µs, *POFFT* at 5 µs, and *PI* at 4 A, supporting the results in Table 4. Fig. 15 shows that in DDTET geometry, the smallest *OC* was achieved with a combination of low *POFFT* and high *PI*. Further reduction in *PI* and *POFFT* also resulted in smaller *OC* values. Additionally, a combination of low *PONT* and low *PI* produced smaller *OC* values, but an increase in *PI* with low *PONT* led to significant response outcomes. A combination of low *POFFT* and low *PONT* also minimized *OC* values. In summary, the significant input values for achieving smaller *OC* values in *DDTET* geometry are low-level POFFT at 5 µs, low PONT at 3 µs, and either high 7 µs or low 4 µs PI values.

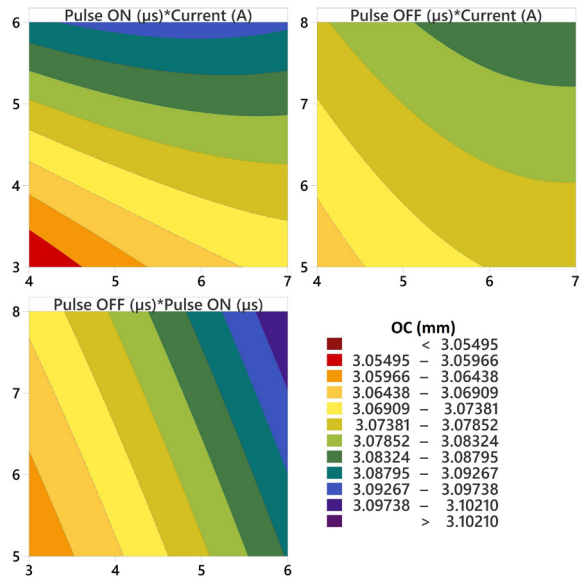

Fig. 14. *OC Surface plot of TET geometry*

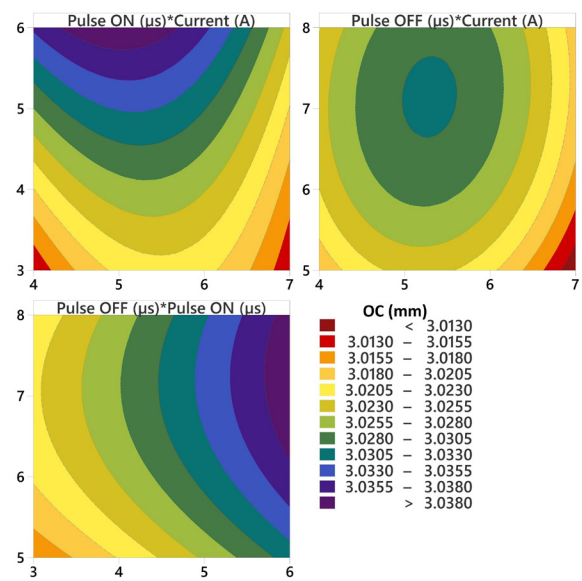

Fig. 15. *OC Surface plot of DDTET geometry*

3.6 Selective Electron Microscope (SEM) Image Analysis

SEM images captured with ZEISS SEM equipment analysed the *RL* and *HAZ* in TET and DDTET geometries. In this instance, the boundary of the RL was indicated in red, while the *HAZ* was marked in yellow. Fig. 16 shows that the 4th and 5th RO in TET geometry have a high *RL* thickness and significant HAZ compared to the *RL* and *HAZ* in DDTET geometry. Fig. 17b, indicates that in RO 5 of the DDTET geometry, a wider gap between the tool and work-piece results in no *RL* formation but a notable *HAZ*, due to effective electrolyte discharge and quenching effect [23] and [24]. Fig. 17a, shows that in RO 4 of the DDTET geometry, there is minimal *RL* compared to TET geometry, with some patches of *HAZ* caused by high thermal energy from a smaller gap.

4 CONCLUSIONS

- The experimental results demonstrated the significant impact of machining parameters on *MRR* and *OC* for both TET and DDTET geometries. According to the ANOVA analysis, *PONT* was identified as the most influential factor, contributing 51.35 % and 48.58 % to *MRR* in TET and DDTET geometries, respectively. PI contributed 28.77 % to *MRR* in TET and 31.67 % in DDTET, while *POFFT* accounted for 17.95 % in TET and 17.85% in DDTET. These findings highlight the importance of fine-tuning the pulse parameters to maximize *MRR* in different geometries.
- In the 16th experimental run (*7 A, 6 µs, 5 µs), both geometries exhibited improved *MRR* due to the optimal distribution of thermal energy. The greatest variation in MRR, with a difference of 21.66 %, was observed in the 9th run (*6 A, 3 µs, 7 µs), indicating that the electrode gap between the tool and work-piece plays a crucial role in

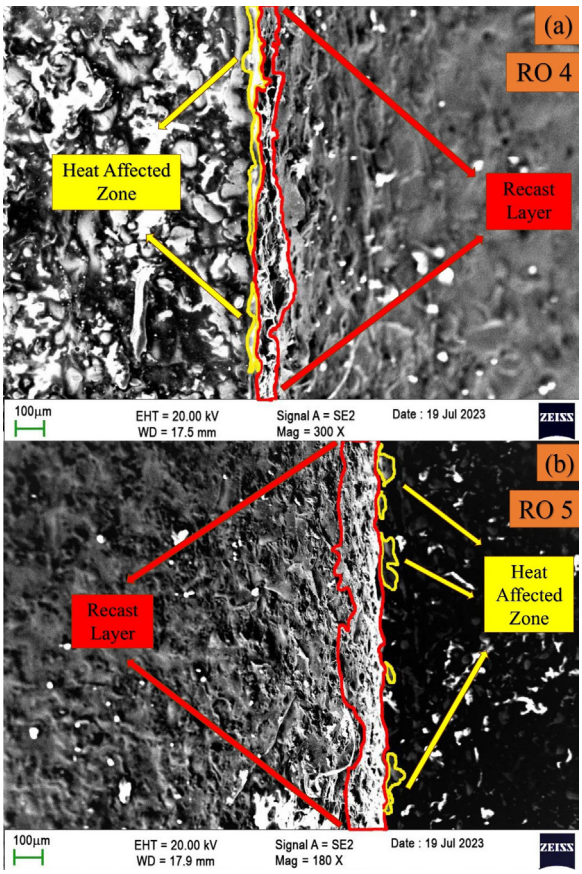

Fig. 16. *a) TET geometry's RL thickness and b) HAZ*

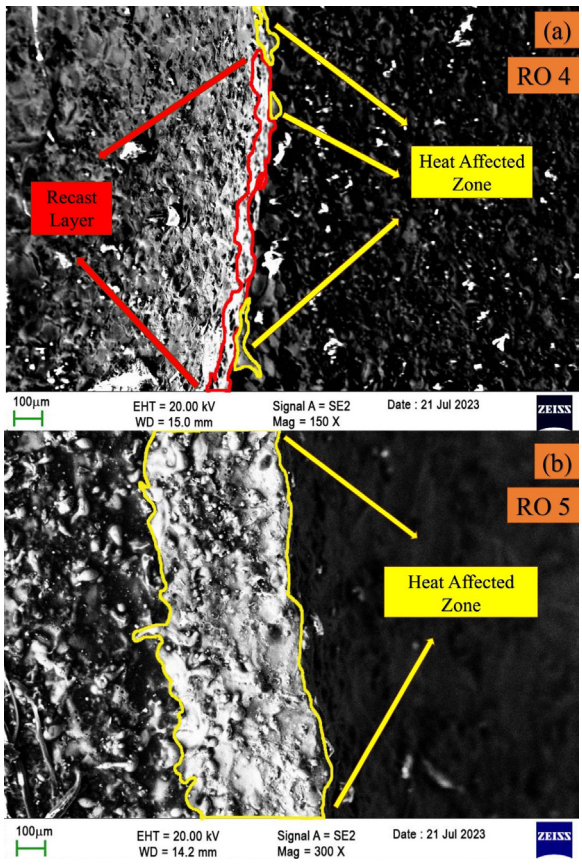

Fig. 17. *a) DDTET geometry's RL thickness and b) HAZ*

MRR differences between TET and DDTET geometries.

- With respect to *OC*, the ANOVA results revealed that *PONT*, *POFFT*, and *PI* contributed 72.25 %, 20.33 %, and 5.33 % in TET, and 47.37 %, 28.37 %, and 23.30 % in DDTET, respectively. The 1st run (*4 A, 3 µs, 5 µs) showed a reduction in *OC* for both geometries, attributed to low *PI*, *PONT*, and *POFFT*, which led to decreased ionization in the machining zone. Moreover, the parameters (*7 A, 3 µs, 5 µs) significantly reduced *OC* values in DDTET geometry, showcasing its potential in achieving minimal dimensional deviation.
- Notably, the 16th run (*7 A, 6 µs, 5 µs) had the highest OC deviation of 2.28 %, which can be attributed to the maximum distance between the tool and work-piece. Furthermore, DDTET geometry exhibited a comparatively thinner *RL* and a smaller *HAZ* than TET geometry, underlining its effectiveness in reducing thermal damage during the machining process.

5 REFERENCES

[1] Kirubagharan, R., Dhanabalan, S., Karthikeyan, T. (2024). The effect of electrode size on performance measures of Inconel X750 using nano-SiC powder mixing electrical discharge machining. *Journal of Materials Engineering and Performance* vol. 33, p. 1283-1303, **DOI:10.1007/s11665-023-08835-z**.

[2] Pal, M.R., Debnath, K., Mahapatra, R.N. (2024). Optimization of machining parameters and analysis of the surface characteristics in micro-electrical discharge machining of 310 and 316 stainless steel. *Journal of Materials Engineering and Performance*, vol. 33, p. 5422-5438, **DOI:10.1007/s11665-024-09192-1**.

[3] Yadav, S., Sisodia, N., Agarwal, D., Singh, R.K., Sharma, A.K. (2024). Performance analysis of powder-assisted micro-drilling operation using micro-EDM. *Proceedings of the Institution of Mechanical Engineers, Part C: Journal of Mechanical Engineering Science*, vol. 238, no. 15, 7627-7639, **DOI:10.1177/09544062241237423**.

[4] Chaudhari, R., Rehman, I.U. Khanna, S., Patel, V.K., Vora, J., Prakash, C., Campilho, R.D.S.G., Al-Sharif, M.S:, Ali, E., Ghoneim, S.S.M. (2024). A parametric study with experimental investigations of expanded graphite on performance measure of EDM process of Ni55.8Ti SMA. *Alexandria Engineering Journal*, vol. 87, p. 164-174, **DOI:10.1016/j.aej.2023.12.013**.

[5] Manikandan, K.P., Thirugnanam, S., Selvarajan, L., Senthilkumar, T S. (2024). Study of correlation of machining performance and geometrical tolerances of Si3N4-TiN composites using EDM process. *Silicon*, vol. 16 p. 3431-3451, **DOI:10.1007/s12633-024-02884-2**.

[6] Shabarinathan, K.T., Senthilkumar, K., Kathiravan, N., Udhayachandran, R.M. (2024). Investigation of enhancing EDM machining performance of INCONEL alloy using composite electrodes. *Materials Research Express*, vol. 11, no. 1, 016513, **DOI:10.1088/2053-1591/ad1b09**.

[7] Sawant, S.N., Patil, S.K., Unune, D.R., Nazare, P., Wojciechowski, S. (2023). Effect of copper, tungsten copper and tungsten carbide tools on micro-electric discharge drilling of Ti-6Al-4V Alloy. *Journal of Materials Research and Technology*, vol. 24, p. 4242-4257, **DOI:10.1016/j.jmrt.2023.04.067**.

[8] Selvarajan, L., Rajavel, R., Arun, C., Raju, C. (2023). Experimental analysis and surface morphology of holes made by electrical discharge machining on MoSi2-SiC composite. *Journal of Materials Engineering and Performance*, **DOI:10.1007/s11665-023-09000-2**.

[9] Rafaqat, M., Mufti, N.A., Saleem, M.Q., Ahmed, N., Rehman, A.U., Ali, M.A. (2023). Machining of triangular holes in D2 steel by the use of non-conventional electrodes in die-sinking electric discharge machining. *Materials*, vol. 16, no. 10, 3865, **DOI:10.3390/ma16103865**.

[10] Rafaqat, M., Mufti, N.A., Saleem, M.Q., Ahmed, N., Rehman, A.U., Zahoor, S., Ali, M.A. (2023). Enhancing electric discharge machining performance by selecting electrode design and geometrical parameters for square, triangular, and hexagonal profiled holes. *Processes*, vol. 11, no. 9, 2661, **DOI:10.3390/pr11092661**.

[11] Kumar, R., Singh, I. (2021). Blind hole fabrication in aerospace material Ti6Al4V using electric discharge drilling: A tool design approach. *Journal of Materials Engineering and Performance*, vol. 30, p. 8677-6885, **DOI:10.1007/s11665-021-06052-0**.

[12] Shah, M.S., Saha, P. (2020). Investigation on performance characteristics of micro-EDM dressing for the fabrication of micro-rod(s) on Ti-6Al-7Nb biomedical material. *Machining Science and Technology*, vol. 25, no. 3, p. 398-421, **DOI:10.1080/10910344.2020.1815050**.

[13] Saha, S., Ball, A.K., Mukherjee, A., Das, A., Halder, S., Hanumaiah, N. (2021). Optimization of electrochemical etching process for manufacturing of micro electrodes for micro-EDM application. *Proceedings of the Institution of Mechanical Engineers, Part B: Journal of Engineering Manufacture*, vol. 235, no. 5, p. 925-940, **DOI:10.1177/0954405420958961**.

[14] Ji, L., Zhang, Y., Wang, G., Zhang, J., Yang, W. (2021). Performance improvement of high-speed EDM and ECM combined process by using a helical tube electrode with matched internal and external flushing. *The International Journal of Advanced Manufacturing Technology*, vol. 117, p. 1243-1262, **DOI:10.1007/s00170-021-07595-1**.

[15] Yadav, V.K., Singh, R., Kumar, P, Dvivedi, A. (2021). Performance enhancement of rotary tool near-dry EDM process through tool modification. *Journal of the Brazilian Society of Mechanical Sciences and Engineering*, vol. 43, 72, **DOI:10.1007/s40430-021-02806-y**.

[16] Jabbaripour, B., Sadeghi, M.H., Faridvand, Sh., Shabgard, M.R. (2012). Investigating the effects of EDM parameters on surface integrity, MRR and TWR in machining of Ti-6Al-4V. *Machining Science and Technology*, vol. 16, no. 3, p. 419-444, **DOI:10.1080/10910344.2012.69897**.

[17] Lo, J.S., Deng, C.S., Jiang, C.T., Lu, C.H. (2019). Slotted electrodes for the improvement of machining performances in EDM drilling. Journal of the Chinese Institute of Engineers,

vol. 42, no. 5, p. 401-410, **DOI:10.1080/02533839.2019.1599300**.

[18] Malayath, G., Sidpara, A.M., Deb, S. (2020). Fabrication of micro-end mill tool by EDM and its performance evaluation. *Machining Science and Technology*, vol. 24, no. 2, p. 169-194, **DOI:10.1080/10910344.2019.1636269**.

[19] Sagar, K.G, Anjani, P.K., Raman, M.S., Latha Devi, N.S.M.P., Mehta, K., Gonzales, J.L.A., Kumar, N.M., Venkatesan, S. (2022). Improving sustainability of EDM sector by implementing unconventional competitive manufacturing approach. *Advances in Materials Science and Engineering*, vol. 2022, p. 6164599, **DOI:10.1155/2022/6164599**.

[20] Dinesh Krishnaa, S., Sangeeth Kumar, M., Dhiyaneswaran, J., Rishi Karthikeyan, V.P, Rithik, B.S. (2024). Irradiation with high energy electron beams increases the hardness of metamorphic copper-based alloys. *SAE Technical Paper*, vol. 2023, **DOI:10.4271/2023-01-5131**.

[21] Kaliappan, S., Pravin., P., Saravanan, K.G., Thanigaivelan, R. (2024). Development and performance optimization of ECM parameters on scrapped alloy wheel metal matrix composites. *High Temperature Material Processes: An International Quarterly of High-Technology Plasma Processes*, vol. 28, no. 2, p. 33-43, **DOI:10.1615/HighTempMatProc.2023048114**.

[22] Kumaravel, P., Suresh, P., , V.K., Raja, Sekar, T. (2022). Improvement of micro-electrochemical discharge machining of austenitic stainless steel 316L using NaOH electrolyte containing N2. *International Journal of Electrochemical Science*, vol. 17, no. 7, 220747, **DOI:10.20964/2022.07.53**.

[23] Duraisivam, S., Suresh, P., Jamuna, E., Prakash, R. (2022). Novel synthesizing and optimization of EDM for electrode wear rate and metal removal rate of copper metal matrix composite reinforced with tungsten carbide. *AIP Conference Proceedings*, vol. 2460, 050003, **DOI:10.1063/5.0096370**.

[24] Scribd HQ. scribd, from *https://www.scribd.com/document/616918290/Stainless-Steel-Grade-202-UNS-S20200*, accessed on 2024-06-20.